Study of Mixing Enhancement of The 3-D Acoustofluidic Mixer using Digital In-Line Holographic Micro-Particle Tracking Velocimetry

Olivia Christy Tarigan[1], . Chen-Chia Li[1], Chia-Kai Chang1, W. H. Tien[1,*]

1: Dept. of Mechanical Engineering, National Taiwan University of Science and Technology
* Correspondent author: whtien@mail.ntust.edu.twy

Keywords: DIHM, Holography, Microfluidics, Acoustofluidics, Micro PTV

ABSTRACT

In this study, the 3-D flow patterns and mixing performances are investigated for an acoustofluidic Y-junction micromixer using Digitial In-line Holographic Micro-Particle Tracking Velocimetry (DIHμPTV) and epi-fluorescence flow visualization. Two parallel longitudinal spines were placed in the channel to induce sustaining solenoidal 3-D acoustic streaming vortices, which work as the secondary flow in the mixing channel to reduce the diffusion mixing length and in turn enhance the mixing performances. The two spines have a triangular cross-section, with a base width of 0.2mm and a height of 0.3mm, placed 1.2mm apart from each other in a 2.8mm width and 1mm height channel. The Y-junction has two configurations, one has the spines directly connected to the side wall at the Y-junction, and the other microchannel has a gap between the two spines and a flat junction shape. The driving mechanism is provided by two piezoelectric disks, operating at 12 kHz oscillation frequency and 20V peak-to-peak amplitude. The 3-D flow patterns were recorded by the DIHμPTV in two measurement volumes to fully cover the test section's height. The holographic reconstruction scheme is based on the 1st Rayleigh-Sommerfeld solution with an extra deconvolution step to improve the accuracy of the reconstruction of the depth position. The deconvolution step utilizes a simulated hologram of the Point-Spread Function (PSF) and reduces the depth uncertainty during the deconvolution of the raw data. The mixing performances of the acoustofluidic Y-junction micro-mixers were evaluated by the epi-fluorescence experiments, and the mixing indices were calculated and compared to verify the improvements compared to the Y-junction micromixers without the acoustic streaming vortices. The results confirmed the improvement of the mixing and the sustaining 3-D flow patterns even with a high flow rate, which could not be achieved with 2-D sharp-edge obstructions tested previously. The novel configuration may have the potential to inspire designs of high-throughput and low-pressure loss active micro-mixers.

1. Introduction

Active micromixers utilize various external energy sources to disturb the fluid and increase the contact area, a phenomenon that aids and enhances fluid mixing. They are designed to achieve homogeneous and rapid mixing in small volumes or at micro scales. They are critical for various

applications such as drug delivery, chemical processing industries, biomedical diagnostics, etc. Acoustic streaming (AS) is one of the mechanisms used by active micromixers that utilizes the power of sound waves to manipulate the microscopic fluid flow. The propagation of sound waves in a fluid induced by high-frequency acoustic oscillations is the spatial and temporal variations of the pressure field, resulting in nonlinear and time-averaged effects. It generates interactions at solid-liquid interfaces in a flow channel and causes a steady streaming flow. Due to its non-contact nature and ease of operation, acoustic streaming is widely used in mixing, sorting, and collecting particles and cells in flow fields[1, 2].

One of the common configurations to induce AS is a 2-D extruded geometry on the sidewall of a microchannel, which induces a pair of counter-rotating acoustic vortices on both sides of the tip under high-frequency oscillations, and the acoustic vortices will change with different top angles and driving voltages [3-6]. In more recent studies, the particle trajectories in microchannels with more complex structures show a richer behavior and are not limited to 2-D flow[7, 8].

The longitudinal spine with tip structure attached to the top wall of the microfluidic channel can induce a 3-D flow pattern of the AS, and the tips of the two longitudinal spines will be different due to the distance between them, which affects the size of the velocity of the acoustic jet. Tarigan [9] used a holographic microscopy method to visualize the 3-D AS flow pattern around the longitudinal spine. The longitudinal spine oscillates to produce two counter-rotating acoustic vortices with a maximum velocity of 300 μm/s. The effect of two parallel longitudinal spines on the AS is also observed at different tip spacing, and it was found that increasing the spacing reduces the mutual interference of the acoustic vortices and provides more space for the development of each AS region.

Among all of the volumetric methods to visualize 3-D microscopic flow, Digital In-line Holographic Microscopy (DIHM) is less hardware-demanding. In the most common configurations, it only requires a typical microscope with a coherent laser light source. The diffraction patterns of all the objects to be imaged are recorded as a hologram, and a reconstruction scheme digitally refocuses the hologram at different depths to generate a set of holographic reconstruction images to identify the objects' 3-D position or profile. The technique was first proposed by Gabor[10], which utilized a spherical reference light wave of known amplitude and phase to interfere with the transmitted wave formed by the illuminated object, and a digital camera to record the interfered pattern, i.e., the hologram. Other advantages of DIHM include the ability to capture the information of the object at several different depths with high resolution without refocusing on a single hologram and a large depth of field. This technique is applied to analyze the 3-D structure of micrometer-sized objects or microorganisms[11, 12], as well as to study the displacements of micro-objects in fluids and analyze the 3-D trajectories to represent the

distribution of the flow field of the fluids in the microfluidic channel[13]. In the field of microfluidic devices, DIHM can be used as a volumetric particle-tracking method to measure the motion of μm-size objects. Sheng et al [6] used the DIHM technique to measure solutions containing 3.2 μm and 0.75 μm polystyrene particles in a 1 mm deep container to obtain the 3D distribution of the particles. Other studies demonstrated the use of DIHM in applications in visualizing the motion of algal cells under free-swimming conditions[14] and the motions of blood cells[15].

Digital In-Line Holographic Particle Tracking Velocimetry (DIHμ-PTV) utilizes the DIHM technique to reconstruct the 3-D locations of the tracer particles and uses the PTV algorithm to further analyze the 3-D velocity vector fields to study the flows. In prior studies, the technique has been validated by simple flow conditions such as steady flow in a semicircular microfluidic channel [16], and a micro-circular tube with different particle volume ratios and flow rates[17]. Hong [18] proposed this algorithm based on DIHM and applied it to measure the three-dimensional flow field of an AS induced by a triangular microstructure in a microfluidic channel. It is found that the induced AS vortices at the tip of the structure have a speed 10 times larger than those on the far side of the tip. Compared to other volumetric method such as Digital Defocusing Micro-Particle Tracking Velocimetry (DDμ-PTV), the DIHμ-PTV system has a much lower demand on the illumination intensity and a larger dynamic range for velocity measurements[19]. One of the problems shared in common with the volumetric methods is the higher uncertainty of the out-of-plane component, and it is more severe for a DIHM-based system due to its large depth of field. Due to the small numerical aperture of the setup, when the 3-D reconstruction is performed, the depth-of-focus signals of the particles along the Z-direction are stretched, resulting in an increase in Z-axis inaccuracy as explored by prior studies[20, 21]. Several solutions have been developed to increase the accuracy of particle position measurement[22, 23]. In these methods, Latychevskaia and Fink proposed a 3-D deconvolution method that can increase the accuracy of the Z-position in reconstructing the 3-D particle position. By reconstructing the simulated hologram of a point-scattering object to obtain the Point-Spread Function (PSF), the reconstructed wavefront from the reconstructed experimental hologram is used in a 3-D deconvolution operation with the PSF. After the operation, the particles are not only more visible in the reconstructed image but also the depth of focus is much reduced compared with that before the operation, which makes it easier to analyze the particle positions.

In this study, the 3-D AS flow patterns induced by two parallel longitudinal spines in a microchannel are investigated by a modified DIHμ-PTV setup. The 3-D deconvolution method proposed by Latychevskaia and Fink [23] is utilized with a cross-correlation scheme to better identify the reconstructed particle center location to more accurately determine the depth location.

The mixing performances of the acoustofluidic Y-junction micro-mixers are also evaluated by the epi-fluorescence experiments, and the mixing indices were calculated and compared to verify the improvements compared to the Y-junction micromixers without the AS vortices.

2. Experiment Method

Fig. 1 shows the basic concept of holographic reconstruction. Reconstruction of the hologram is based on the theoretical model of reconstruction in the study of Hong [18], using the first solution of Rayleigh-Sommerfeld in the Huygens-Fresnel light propagation principle for the reconstruction of the whole image:

$$U(P) = \frac{1}{i\lambda z'}\int_{y_1}^{y_{jj}}\int_{x_1}^{x_{ii}} U(Q)exp\left(ikz'\sqrt{1+\left(\frac{x-x'}{z'}\right)^2+\left(\frac{y-y'}{z'}\right)^2}\right)dxdy \quad (1)$$

where $U(Q) = \left(\frac{A}{2}\right)\left(\frac{e^{ik\rho}}{\rho'}\right)\cos\theta$ denotes the hologram image located on the recording plane. Equation (1) is converted to the frequency domain by Fourier transformation and then converted back to the spatial domain by Fourier inverse transformation, which is the light field reconstruction equation:

$$\mathcal{F}^{-1}\{\mathcal{F}[U(P)]\} = \mathcal{F}^{-1}\left\{\frac{1}{i\lambda z'}\int_{y_1}^{y_{jj}}\int_{x_1}^{x_{ii}}\mathcal{F}[U(Q)]exp\left[\frac{i2\pi z'}{\lambda}\sqrt{1-(\lambda f_x)^2-\left(\lambda f_y\right)^2}\right]dxdy\right\} \quad (2)$$

Equation (2) is used to program the light-field reconstruction.

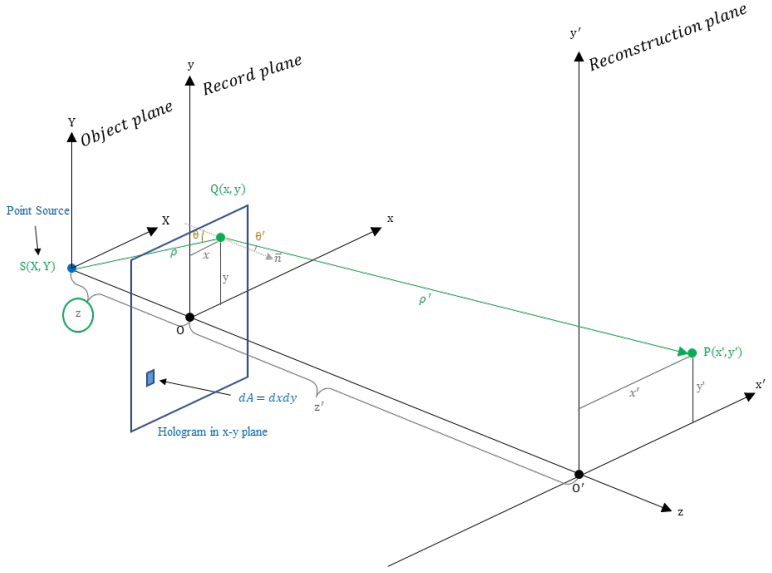

Fig. 1 Basic concept of holographic reconstruction

The deconvolution method finds the maximum of the deconvolution distribution:

$$o(x,y,z) = \mathcal{F}^{-1}\left\{\frac{\mathcal{F}\left[\left|U(P)_{\text{Object}}\right|^2\right]}{\mathcal{F}[|U(P)_{\text{PSF}}|^2 + \beta]}\right\}$$

, which only happens when the reconstructed scatter field of the object matches exactly with the signal from the PSF (Point-Spread Function, including the off-focal plane distribution) of a single-point scatterer. The PSF of this ideal single-pixel, single-point scatterer forms a hologram at distance z is

$$U(P)_{\text{PSF}} = \mathcal{F}^{-1}\left\{\mathcal{F}[U(Q)_{\text{PSF}}]exp\left[-\frac{i2\pi z}{\lambda}\sqrt{1-(\lambda f_x)^2-(\lambda f_y)^2}\right]\right\}$$

To accurately locate each particle's center in the reconstructed plane from the hologram, a 2-D normalized cross-correlation analysis of Lewis [4] is adopted to compare the ideal point scatterer (Fig. 2(a)) and the experimental reconstructed image (Fig. 2(b)), and the normalized correlation coefficient R indicates the degree of similarity of the two images:

$$\mathrm{R}(u,v) = \frac{\sum_{x,y}\left[f(x,y) - \bar{f}_{u,v}\right]\left[t(x-u,y-v) - \bar{t}\right]}{\left\{\sum_{x,y}\left[f(x,y) - \bar{f}_{u,v}\right]^2 \sum_{x,y}[t(x-u,y-v) - \bar{t}]^2\right\}^{0.5}}$$

The result is a correlation matrix R as shown in Fig. 2(c). The peak position corresponds to the position of the reconstructed particle image, and through the reconstructed Z-planes a fitted Z for the maximum of R can be determined. Then the particle's X and Y positions can be determined accurately by a 2-D peak-finding scheme and a magnification conversion at this Z position.

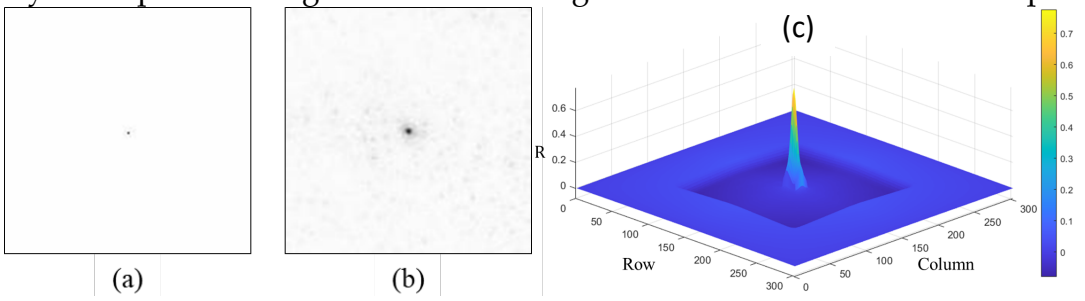

Fig. 2 Deconvolution and cross-correlation method used in the current study: (a) PSF of the ideal point scatterer (b) Real reconstructed particle image at the focal plane (c) The cross-correlation map of (a) and (b)

The experimental setup is shown in Fig. 3. To obtain a 3-D flow field in the microchannel, the DIHμ-PTV system is used to calculate the trajectories of particles. In this setup, an inverted microscope (WHITED, WI-400) is utilized, with a blue laser (λ = 450 nm) as the light source. The laser passes through a 100 μm diameter pinhole to form a spherical wave light source that is transmitted to the microchannel. This illumination causes the particles within the microchannel to produce scattered waves. Additionally, a 20x objective lens and a CMOS camera (MQ013CG-ON, 1280 × 1024 pixels) with a pixel size of 4.8 μm are employed to capture the holograms. An Arduino-

controlled driver circuit is used to synchronize the laser and the camera through the computer, enabling the laser to flash at a specific frequency and capture holograms simultaneously for DIHμ-PTV. In this experiment, the exposure time and frame rate of the camera are 46 ms and 20 fps, respectively.

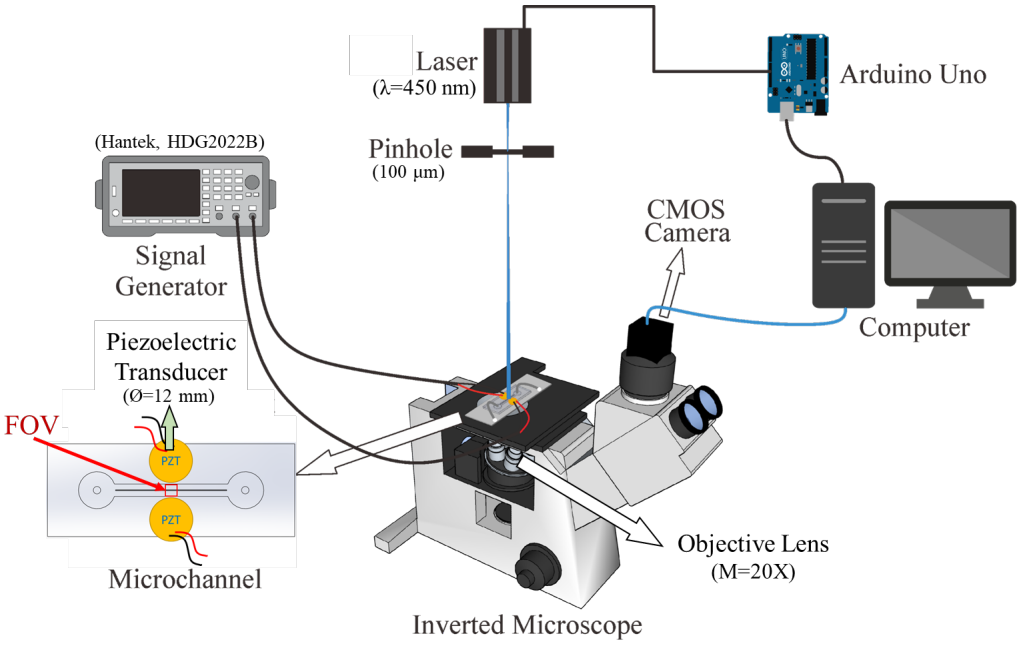

Fig. 3 Experimental setup of the DIHμ-PTV system.

Due to the constraints of the reconstruction depth range, the focal planes were set at depths of 500 μm and 900 μm down from the top of the microchannel for the capture, respectively.

Two post-image processing procedures of the DIHμ-PTV technique are compared. Fig. 4(a) shows data processing flow of the direct reconstruction method adopted from [YiYu Chen], and Fig. 4(b) shows the data-processing flow of the deconvolution reconstruction method developed in the current study. The main difference is that the deconvolution reconstruction method has additional steps to utilize the single-point scatterer PSF for the deconvolution scheme and the cross-correlation scheme to determine the particle image position more accurately.

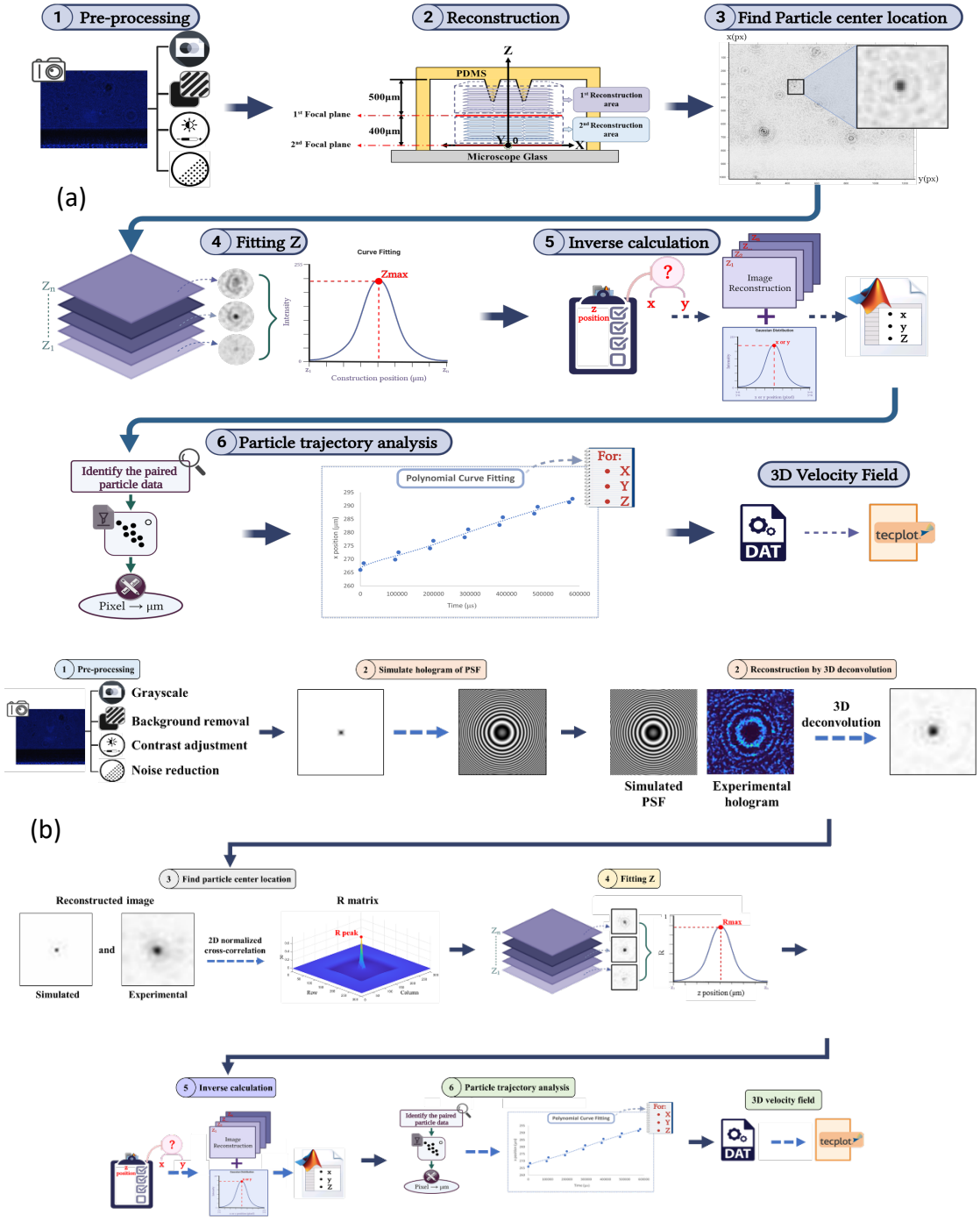

Fig. 4 The process flow of the DIHμ-PTV post-processing: (a) The direct reconstruction, (b) the deconvolution reconstruction.

Fig. 5 shows the two recording regions for using the DIHμ-PTV. The holograms are recorded at these two focal planes (100 and 500μm), respectively, and the reconstruction tasks are also processed separately to obtain a more detailed investigation of these two regions.

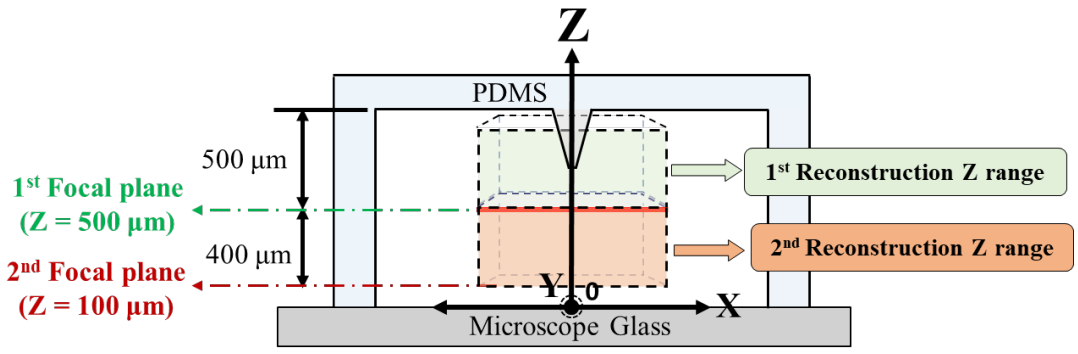

Fig. 5 Schematic of the reconstructed areas in the microchannel.

Fig. 6 shows the design details of the Y-mixer microchannel with two parallel longitudinal spines on its top wall, each longitudinal spine has a tip angle of 30° and is parallel to the direction of fluid flow. Two slightly different spine designs are made and tested in this study, with the main difference being if the spines are connected to the junction part of the Y-mixer channel. A solution containing 1.79um diameter carboxylate fluorescent particles (Polysciences, Fluoresbrite® BB Carboxylate Microspheres 1.75 μm) at a concentration of 10 ppm is injected into the microchannel. Two piezo disks with a diameter of 12mm are glued to both sides of the microchannel on the PDMS surface, and a signal generator provides the signal of sinusoidal waves with a frequency of 12 kHz and voltage up to 30 V to the piezo disks, generating oscillations that induce the 3-D acoustic streaming around the spines, as shown in Fig. 7. The microfluidic devices were made with Polydimethylsiloxane (PDMS) and molded in poly methyl methacrylate (PMMA) molds.

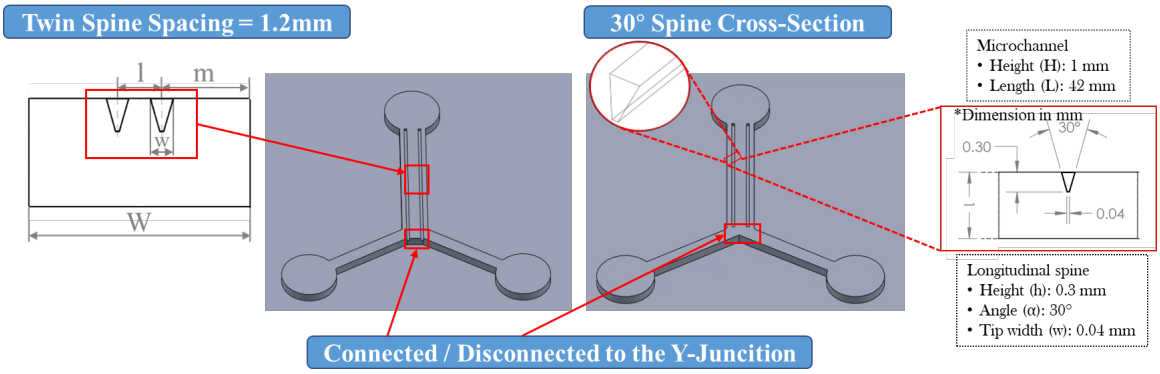

Fig. 6 The two Y-mixer channel designs with longitudinal spine: (a) Spine and Y-junction are connected. (b) The spine with the Y-junction is disconnected

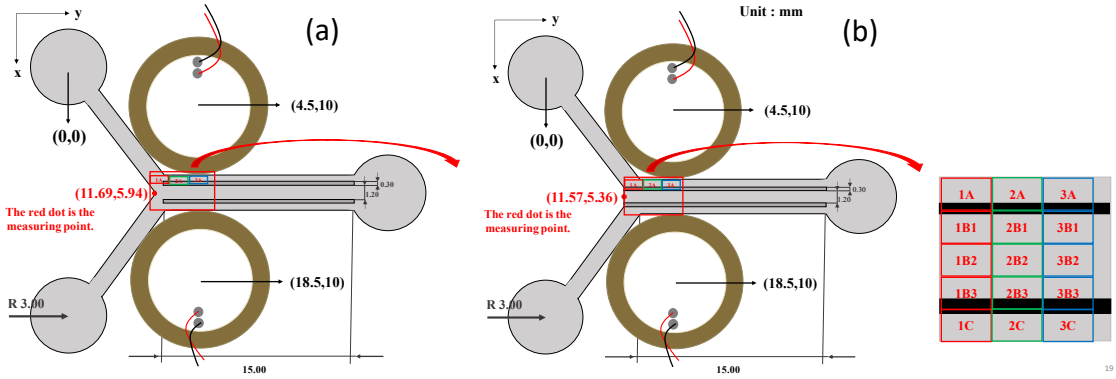

Fig. 7 The schematics of the microfluidic device used in the current study: (a) Spine with the Y-junction is disconnected (b) Spine with the Y-junction is connected

3. Results and Discussion

Fig. 8 compares the calibration results between the direct reconstruction method and the deconvolution reconstruction method in the current study. The mean errors from the planes of the calibration targets are compared at the 1st focal plane at Z=500 μm and the 2nd focal plane at Z=900 μm, respectively. It is found that the mean errors are slightly better at the range of 0 to 400 μm. The slight improvement should be because the deconvolution scheme used in the current method reduces the Z-position uncertainty, but it doesn't eliminate the effect of the refraction index effect of the water on the optical path, which is always present in actual experiments.

Fig. 9 and Fig. 10 show the comparison of the X, Y, and Z position uncertainty between the direct reconstruction method and the deconvolution reconstruction method in the current study. The uncertainties reduce significantly from the direct reconstruction method's $\delta_{\Delta X} = 3.15$ μm, $\delta_{\Delta Y} = 1.11$ μm, $\delta_{\Delta Z} = 14.03$ μm to the deconvolution method's $\delta_{\Delta X} = 1.82$ μm, $\delta_{\Delta Y} = 0.84$ μm and $\delta_{\Delta Z} = 10.29$ μm. The calibration target point can be correctly located per plane increase from 5.56 pt/plane to 7.2 pt/plane. This significant improvement should be mainly because of the implementation of the deconvolution scheme that reduces the Z-position uncertainty during the reconstruction process, but the cross-correlation scheme to identify the particle center more accurately for the refocus of each particle certainly improves the results as well.

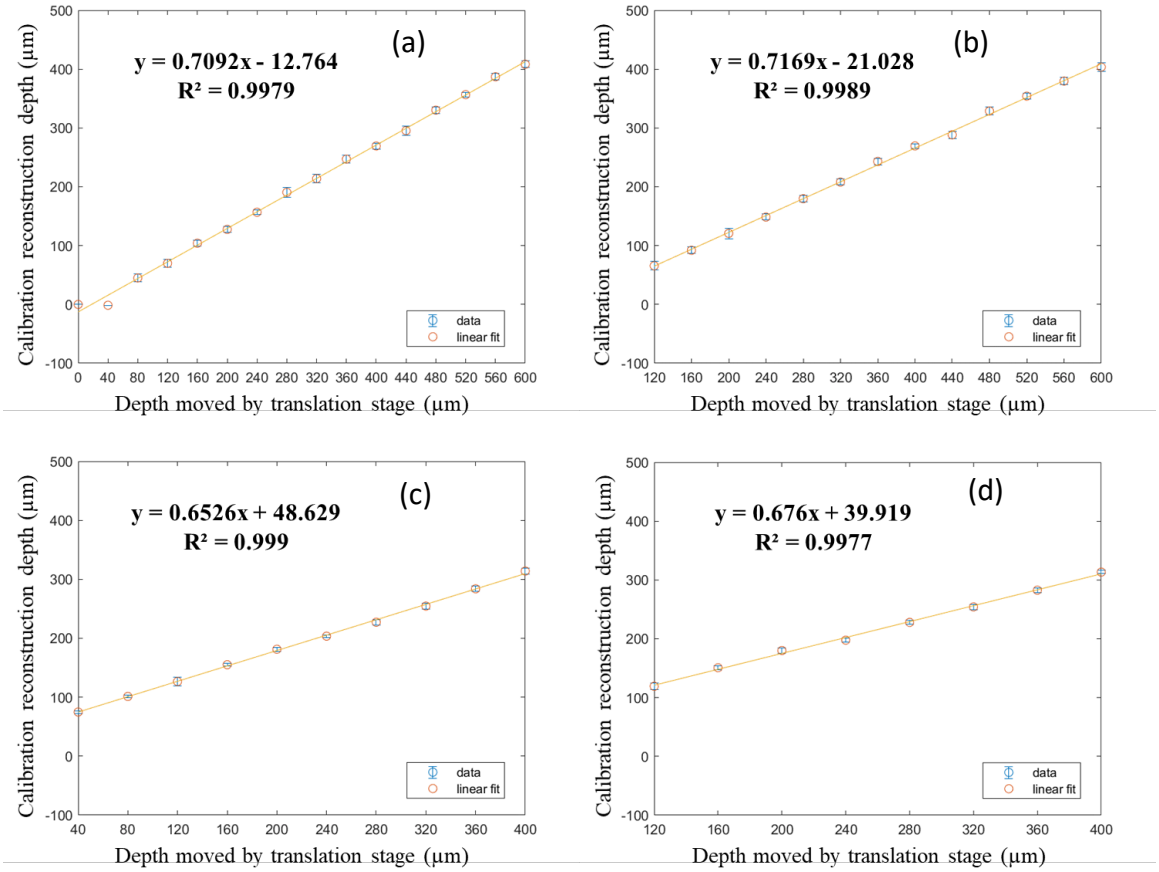

Fig. 8 Mean errors of the calibration results between the reconstruction methods: (a) Focal plane at Z=500 μm (b) Focal plane at Z=900 μm for the direct reconstruction method, and (c) Focal plane at Z=500 μm (d) Focal plane at Z=900 μm the deconvolution reconstruction method in the current study

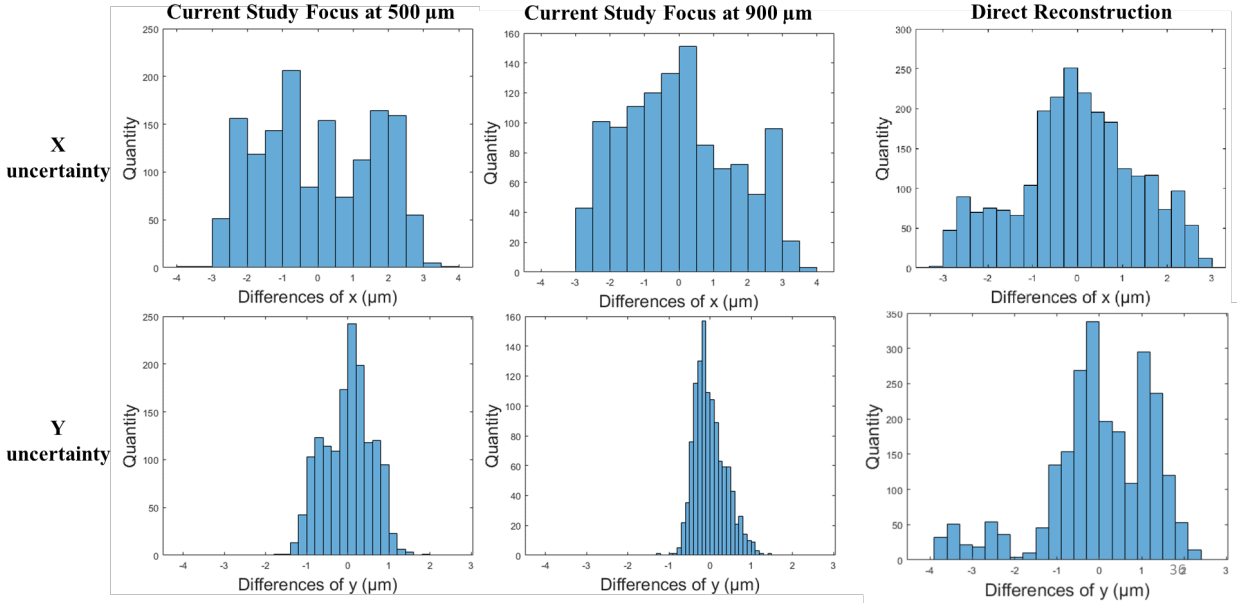

Fig. 9 X and Y position uncertainties of the calibration results between the reconstruction methods.

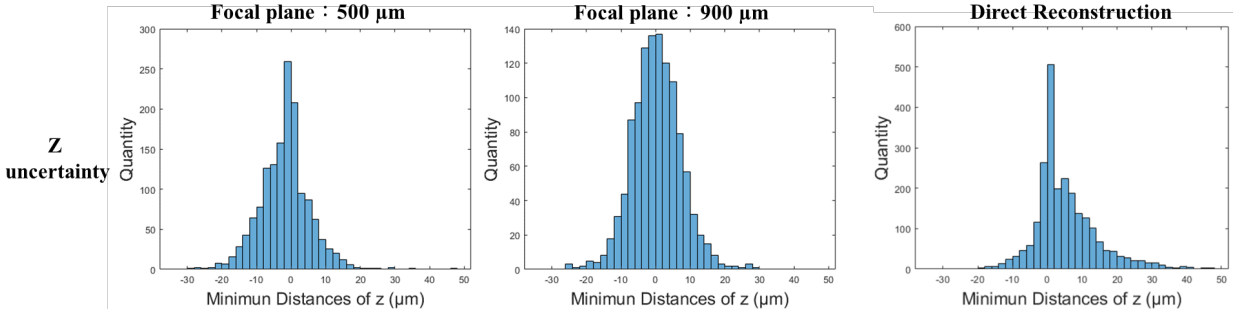

Fig. 10 Z position uncertainties of the calibration results between the reconstruction methods.

Fig. 11 shows the results of the 3-D velocity field for each part of the microchannel. The particle solutions were injected into microchannels with distances of 1.2 mm between the tips of the parallel longitudinal spines. The 3-D distribution of particles and the 3-D velocity field of the fluid for each type were obtained by the DIHμ-PTV system. It can be observed that under high-frequency oscillation applied to the two spines, a pair of counter-rotating acoustic streaming vortices is induced in the area between the spines, and the rotational direction of the vortices is always from the bottom of the spine's tip, flowing upwards towards the outer sides of the two spines. The depth direction of the acoustic streaming exhibits a dynamic range from 500 to 900 μm. The fluid velocity can reach up to 336 μm/s. The results suggest that with the presence of the AS, the rolling motion can create a secondary flow pattern that would be less likely to be interfered with by the axial flow, which is a main issue in the 2-D extrusion-type AS microfluidic device.

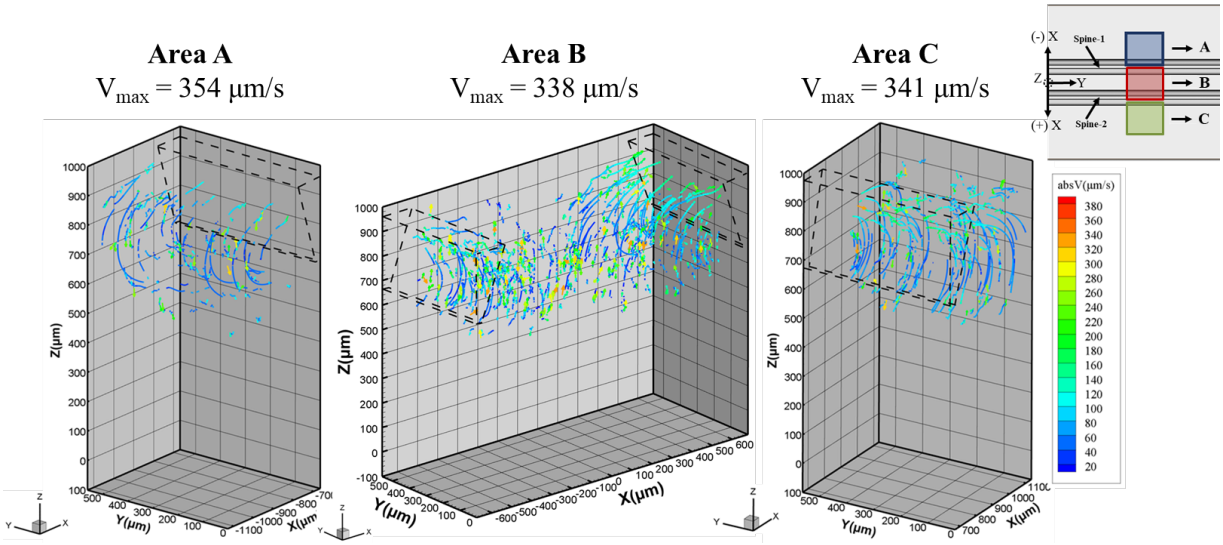

Fig. 7 The 3-D velocity fields of microchannels with 1.2 mm between the tips of the parallel longitudinal spines.

4. Conclusions and Future Works

In this study, the DIHμ-PTV technique was successfully employed to visualize and evaluate the 3-D velocity field of the acoustic streaming in the microchannel. The modified methods in the reconstruction procedure provide significant improvements in the accuracy of determining the particle's 3-D positions, while also increasing the possibility of identifying the particle's image during the reconstruction process. The results show that a pair of counter-rotating acoustic streaming vortices is induced in the area between the parallel longitudinal spines. As the spacing between the spines increases, the interference between the two vortices gradually decreases. When the distance between the tips of the spines is 1.2 mm, the two vortices are symmetrical and separated. Currently mixing experiments are underway to validate the effect of the 3-D AS flow and its effect on the mixing enhancement at different flow rates.

Acknowledgments

The authors would like to acknowledge that this research is sponsored by the Ministry of Science and Technology, Taiwan, R.O.C. under Grant No. 112-2221-E-011 -078 -

References

1. Bachman, H., et al., An acoustofluidic device for efficient mixing over a wide range of flow rates. *Lab on a Chip*, 2020. 20(7): p. 1238-1248.
2. Huang, P.-H., et al., A reliable and programmable acoustofluidic pump powered by oscillating sharp-edge structures. *Lab on a Chip*, 2014. 14(22): p. 4319-4323.
3. Wu, J., Acoustic streaming and its applications. *Fluids*, 2018. 3(4): p. 108.
4. Zhang, C.Y., et al., Acoustic streaming near a sharp structure and its mixing performance characterization. *Microfluidics and Nanofluidics*, 2019. 23(9).
5. Xie, Y.L., H. Bachman, and T.J. Huang, Acoustofluidic methods in cell analysis. *Trac-Trends in Analytical Chemistry*, 2019. 117: p. 280-290.
6. Hao, N.J., et al., Acoustofluidics-Assisted Engineering of Multifunctional Three-Dimensional Zinc Oxide Nanoarrays. *Acs Nano*, 2020. 14(5): p. 6150-6163.
7. Marin, A., et al., Three-Dimensional Phenomena in Microbubble Acoustic Streaming. *Physical Review Applied*, 2015. 3(4).
8. Muller, P.B., et al., Ultrasound-induced acoustophoretic motion of microparticles in three dimensions. *Physical Review E*, 2013. 88(2).
9. Olivia Christy, T., *數位同軸全像微粒循跡測速儀用於研究微流道中縱向脊柱誘發的 3-D 流動型態*, in 機械工程系. 2023, 國立臺灣科技大學: 台北市. p. 136.
10. Gabor, D., A New Microscopic Principle. *Nature*, 1948. 161(4098): p. 777-778.

11. Yu, X., et al., Review of digital holographic microscopy for three-dimensional profiling and tracking. *Optical Engineering*, 2014. 53(11).

12. Garcia-Sucerquia, J., et al., Digital in-line holographic microscopy. *Applied Optics*, 2006. 45(5): p. 836-850.

13. Tian, L., et al., Quantitative measurement of size and three-dimensional position of fast-moving bubbles in air-water mixture flows using digital holography. *Applied Optics*, 2010. 49(9): p. 1549-1554.

14. Sohn, M.H., et al., Determination of the swimming trajectory and speed of chain-forming dinoflagellate Cochlodinium polykrikoides with digital holographic particle tracking velocimetry. *Marine Biology*, 2011. 158(3): p. 561-570.

15. Garcia-Sucerquia, J., et al., 4-D imaging of fluid flow with digital in-line holographic microscopy. *Optik*, 2008. 119(9): p. 419-423.

16. Satake, S., et al., Three-dimensional flow tracking in a micro channel with high time resolution using micro digital-holographic particle-tracking velocimetry. *Optical Review*, 2005. 12(6): p. 442-444.

17. Kim, S. and S.J. Lee, Measurement of 3D laminar flow inside a micro tube using micro digital holographic particle tracking velocimetry. *Journal of Micromechanics and Microengineering*, 2007. 17(10): p. 2157-2162.

18. 洪聖博, *數位同軸全像微粒循跡測速儀之研發與其於聲射微流體之應用*, in 機械工程系. 2022, 國立臺灣科技大學: 台北市. p. 162.

19. 陳弈瑀, *數位離焦微粒循跡測速儀與數位同軸全像微粒循跡測速儀用於量測聲射微流體裝置之三維流場之性能比較*, in 機械工程系. 2022, 國立臺灣科技大學: 台北市. p. 118.

20. Murata, S. and N. Yasuda, Potential of digital holography in particle measurement. *Optics and Laser Technology*, 2000. 32(7-8): p. 567-574.

21. Sheng, J., E. Malkiel, and J. Katz, Digital holographic microscope for measuring three-dimensional particle distributions and motions. *Applied Optics*, 2006. 45(16): p. 3893-3901.

22. Pan, G. and H. Meng, Digital holography of particle fields: reconstruction by use of complex amplitude. *Applied Optics*, 2003. 42(5): p. 827-833.

23. Latychevskaia, T. and H.W. Fink, Holographic time-resolved particle tracking by means of three-dimensional volumetric deconvolution. *Optics Express*, 2014. 22(17): p. 20994-21003.